Available online at www.sciencedirect.com
SCIENCE DIRECT®
Sensors and Actuators B 96 (2003) 451–459
SENSORS AND ACTUATORS B CHEMICAL
www.elsevier.com/locate/snb

Measurement of particle size distribution in suspension polymerization using in situ laser backscattering

Eric J. Hukkanen, Richard D. Braatz*

Department of Chemical and Biomolecular Engineering, University of Illinois at Urbana-Champaign, 600 South Mathews Avenue, 93 Roger Adams Laboratory, Box C-3, Urbana, IL 61801-3792, USA

Received 31 July 2002; accepted 2 July 2003

Abstract

Many methods have been developed for characterizing the particle size distribution (PSD) in a suspension polymerization reactor, but are restricted to suspensions with low volume fractions of polymer or to determining the PSD only at the end of the batch. Laser backscattering can be used to measure the chord length distribution for slurries with high particle densities. Here, a combination of inverse modeling and laser backscattering is used to determine the PSD for polymer beads typical of operations for a suspension polymerization reactor. Several methods are compared for accurately determining the PSD from the reported chord length distribution (CLD), including methods that take surface roughness into account. These results demonstrate the applicability of laser backscattering for the in situ particle size distribution analysis in suspension polymerization reactors.

Keywords: Laser backscattering; FBRM; Particle size distribution; Chord length distribution; Particle size analysis; Suspension polymerization

1. Introduction

The particle size distribution (PSD) in suspension polymerization reactors has a direct effect on the product quality. In situ measurements of the PSD would improve the quality of process models, which should have a subsequent effect on improving the optimization and control of suspension polymerization reactors. Existing techniques, while informative for some systems, have significant limitations. In particular, most methods have long time delays before the measurements of the PSD are available. These delays can be the result of the sample preparation or the actual measurement itself [18].

Different methods for particle size analysis are applicable to different size ranges of the particles. A common off-line method to measure the PSD for solid particles is sieving. This technique does not have sampling problems, in terms of obtaining a representative sample, since a large amount of material can be used. A weakness of this method is that it does not have good resolution. Generally, sieving can measure particle size no smaller than ∼38 μm. Particles can also be measured by the sedimentation method, such as Sedi-Graph, in which particles of different sizes fall at different rates through a fluid of known viscosity. The minimum size of the particle measured by sedimentation is ∼2 μm. Centrifugation is a method for particle size analysis that separates particles by the response of physical forces acted upon the particles as a function of the particle size. The minimum size obtained by centrifugation is ∼0.05 mm. All three methods are strongly influenced by the particle shape. Although these methods are relatively simple to use and inexpensive, none of these methods are on-line measurements which can be used for control of the PSD. These techniques are used for final particle size analysis [20,34].

There is a strong advantage to have an *on-line* measurement of the PSD, both in terms of providing more data for modeling purposes, but also to enable on-line optimization and feedback control. Over the years, several particle size analyzers have become available. The Coulter Counter [1] counts particles electronically as the slurry passes through an orifice. Coulter Counters have small flow orifices that are prone to clogging, in the case of high density crystal slurries, and may require grounding of the fluid to reduce background noise [30].

Forward light scattering is an approach for particle sizing commonly used in academic research laboratories. A laser beam is directed through a sample cell and the scattered light is collected. Scattered light is collected from a laser beam

* Corresponding author. Tel.: +1-217-333-5073; fax: +1-217-333-5052.
E-mail address: braatz@uiuc.edu (R.D. Braatz).

0925-4005/$ – see front matter © 2003 Elsevier B.V. All rights reserved.
doi:10.1016/S0925-4005(03)00600-2

directed through a sample cell. The Malvern or Microtrac particle sizes give useful PSD measurements for slurries with low particle density [12,13,27]. Denser slurries can be addressed with an automatic sampling and dilution unit [17], but it can be difficult to obtain a representative sample for such systems. Forward light scattering has been used in several polymer systems [4–9,24,25,29,35].

Other on-line particle size analyzers include ultrasonic extinction, such as the Sympatec Opus, and in situ video microscopy, such as the Lasentec process video microscope (PVM) and the MTS Particle Image Analyzer [15,19]. Ultrasonic extinction can measure particles from 0.01 to 3000 μm [23]. A weakness of video microscopy is that particles smaller than ∼3 μm cannot be observed in solution, and particles near that size range are blurry and difficult to accurately size. These instruments are not as widely used in polymerization systems.

An alternative light scattering approach is to focus a laser beam forward through a window in a probe tip, and collect the laser light scattered back to the probe. The Par Tec 100 was one of the first commercial instruments of this type. This probe and the Lasentec focused beam reflectance measurement (FBRM) probe have been used to investigate the PSD during industrial crystallization processes [3,14,16,22,33]. More recently, the FBRM probe has been used in emulsion and suspension polymerization systems [10,11], but has been limited to determination of mean chord length sizes. Here, we demonstrate the on-line measurement of the PSD in suspension polymerization reactors using an FBRM probe coupled with inverse modeling.

2. Theory

The FBRM probe measures the chord length distribution (CLD) as the laser beam emitted from the sensor crosses particles that pass within its focal point, with the chord length being the distance for which the laser beam crosses a particle. The probe measures thousands of chord lengths per second. There have been efforts to relate the CLD to the PSD [2,21,31,32]. Here, the resolution of past approaches is improved by considering more carefully the character of the PSD.

The measured chord lengths are collected in n bins to form the CLD,

$$\boldsymbol{c} = \begin{pmatrix} c(D_1, D_2) \\ \vdots \\ c(D_n, D_{n+1}) \end{pmatrix} \tag{1}$$

where $c(D_j, D_{j+1})$ is the number of chords within a bin with a size range

$$D_j \leq D < D_{j+1} \tag{2}$$

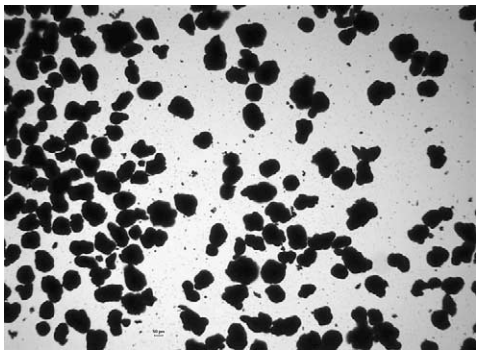

Fig. 1. Off-line optical microscopy picture of poly(vinyl chloride) particles.

The PSD, $\boldsymbol{f}$, is represented by

$$\boldsymbol{f} = \begin{pmatrix} f(D_1, D_2) \\ \vdots \\ f(D_n, D_{n+1}) \end{pmatrix} \tag{3}$$

where each element represents the number of particles within the range (2) and the upper and lower bounds are the bin edges.

The particles are assumed to be spheres, which is a reasonable assumption for suspension polymerization reactors (shown in Fig. 1). The CLD is related to the PSD through probability functions [2,21,31,32]. The probability of a measured chord length being in a particular range is determined. This probability function is constructed for each particle size and the corresponding chord lengths in a matrix that maps the PSD onto the CLD:

$$\boldsymbol{c} = \boldsymbol{P}\boldsymbol{f} \tag{4}$$

where the elements of $\boldsymbol{P}$ are described by the equations

$$P_i(\hat{D}_j) = \begin{cases} \sqrt{1 - \left(\dfrac{D_i}{\hat{D}_j}\right)^2} - \sqrt{1 - \left(\dfrac{D_{i+1}}{\hat{D}_j}\right)^2}, & i < j \\ \sqrt{1 - \left(\dfrac{D_i}{\hat{D}_j}\right)^2}, & i = j \\ 0, & i > j \end{cases} \tag{5}$$

for a single spherical particle of size $\hat{D}_j \in [D_j, D_{j+1})$.

If $D_1 = 0$ then

$$\sum_{i=1}^{n} P_i(\hat{D}_j) = 1 \quad \text{for} \quad j = 1, \ldots, n, \tag{6}$$

that is, the probability of measuring a chord length of a particle is 1.

The above theory is a generalized view of constructing the mapping matrix, $\boldsymbol{P}$, since there has been no mention of how the variable $\hat{D}_j$ is selected. The only constraint is that the

particle diameter lies within each bin. This paper considers several approaches for defining the particle diameter, $\hat{D}_j$, some of which can give more accurate estimates of the PSD than past methods. These approaches are based on the assumption being made on how particles are distributed within each bin, with these distributions being midpoint, uniform, and linear.

2.1. Midpoint distribution

This distribution assumes that, within each bin of size range

$$D_j \le D < D_{j+1}, \tag{7}$$

all of the particles with measured chord lengths have a particle diameter size of

$$\hat{D}_j = \tfrac{1}{2}(D_j + D_{j+1}), \tag{8}$$

which is the midpoint of the bin. In this case, (5) becomes

$$P_{ij} = \begin{cases} \sqrt{1-\left(\dfrac{2D_i}{D_j+D_{j+1}}\right)^2} - \sqrt{1-\left(\dfrac{2D_{i+1}}{D_j+D_{j+1}}\right)^2}, & i < j \\ \sqrt{1-\left(\dfrac{2D_i}{D_j+D_{j+1}}\right)^2}, & i = j \\ 0, & i > j \end{cases} \tag{9}$$

2.2. Uniform distribution

In this approach, it is assumed that within each bin, the size of the particles are uniformly distributed. The general formula for this approach is

$$P_{ij} = \begin{cases} \dfrac{\int_{D_j}^{D_{j+1}} (\sqrt{1-(D_i/D)^2} - \sqrt{1-(D_{i+1}/D)^2})\,\mathrm{d}D}{D_{j+1}-D_j}, & i < j \\ \dfrac{\int_{D_j}^{D_{j+1}} \sqrt{1-(D_i/D)^2}\,\mathrm{d}D}{D_{j+1}-D_j}, & i = j \\ 0, & i > j \end{cases} \tag{10}$$

The integrals are solved analytically to reduce computation time.

2.3. Linear distribution

This approach assumes that, within each bin, the particles are distributed according to the linear equation

$$f(D) = \frac{f(D_{j+1}) - f(D_j)}{D_{j+1} - D_j}(D - D_j) + f(D_j) \tag{11}$$

This assumes that the PSD is continuous, which is expected for suspension polymerization reactors since the polymer particles began as droplets dispersed by a mixing blade. In this case, each element of the mapping matrix is given by

$$P_{ij} = \begin{cases} \dfrac{\int_{D_j}^{D_{j+1}} f(D)(\sqrt{1-(D_i/D)^2} - \sqrt{1-(D_{i+1}/D)^2})\,\mathrm{d}D}{\int_{D_j}^{D_{j+1}} f(D)\,\mathrm{d}D}, & i < j \\ \dfrac{\int_{D_j}^{D_{j+1}} f(D)\sqrt{1-(D_i/D)^2}\,\mathrm{d}D}{\int_{D_j}^{D_{j+1}} f(D)\,\mathrm{d}D}, & i = j \\ 0, & i > j \end{cases} \tag{12}$$

For practical PSDs, this distribution would be expected to be more accurate than the uniform and midpoint distributions, which have been assumed in past studies.

2.4. Inverse modeling

For the uniform and midpoint methods, the PSD can be calculated as the solution to

$$\min_{\boldsymbol{f}} \tfrac{1}{2}(\boldsymbol{P}\boldsymbol{f} - \boldsymbol{c})^{\mathrm{T}}(\boldsymbol{P}\boldsymbol{f} - \boldsymbol{c}) \tag{13}$$

It can be shown that the mapping matrix $\boldsymbol{P}$ is nonsingular for the midpoint and uniform distributions, so there is a unique PSD for a given CLD that is computed using matrix inversion $\boldsymbol{f} = \boldsymbol{P}^{-1}\boldsymbol{c}$. However, the PSD computed by direct matrix inversion can have nonphysical fluctuations (and sometimes even negative values) due to measurement noise and poor conditioning of the mapping matrix. This problem can be avoided by using ridge regression [28]:

$$\boldsymbol{f} = (\gamma \boldsymbol{I} + \boldsymbol{P}^{\mathrm{T}}\boldsymbol{P})^{-1}\boldsymbol{P}^{\mathrm{T}}\boldsymbol{c} \tag{14}$$

where the variable γ is selected to be some small positive number. Using this method, there is a trade-off between bias and matrix conditioning. For large values of γ (for example, equal to 1), the matrix $(\gamma \boldsymbol{I} + \boldsymbol{P}^{\mathrm{T}}\boldsymbol{P})$ is well-conditioned but the calculated PSD is highly biased (it is flatter than the true PSD). For smaller γ, there is less bias but the matrix is more poorly conditioned. In practice, γ is selected to be just large enough that the calculated PSD looks reasonable (e.g. the distribution is smooth). Ridge regression is probably the most commonly used method for inverse modeling.

The mapping matrix for the linear method is a function of the PSD, that is

$$\boldsymbol{c} = \boldsymbol{P}(\boldsymbol{f})\boldsymbol{f} \tag{15}$$

so the mapping between $\boldsymbol{f}$ and $\boldsymbol{c}$ is nonlinear. We propose to compute the PSD by numerical solution of the nonlinear constrained optimization program

$$\min_{\boldsymbol{f}} \tfrac{1}{2}[\boldsymbol{P}(\boldsymbol{f})\boldsymbol{f} - \boldsymbol{c}]^{\mathrm{T}}[\boldsymbol{P}(\boldsymbol{f})\boldsymbol{f} - \boldsymbol{c}] + \hat{\gamma}\boldsymbol{f}''^{\mathrm{T}}\boldsymbol{f}'' \tag{16}$$

subject to

$$\boldsymbol{f} \ge 0 \tag{17}$$

where

$$\boldsymbol{f}'' = \begin{pmatrix} -2 & 1 & 0 & \dots & 0 \\ 1 & -2 & 1 & 0 & \vdots \\ 0 & \ddots & \ddots & \ddots & 0 \\ \vdots & 0 & 1 & -2 & 1 \\ 0 & \dots & 0 & 1 & -2 \end{pmatrix} \boldsymbol{f} \tag{18}$$

using sequential quadratic programming (SQP) (in this case, the program FFSQP [37]). For nonzero $\hat{\gamma}$, the second term in the objective of (16) directly penalizes fluctuations in the distribution, as discussed in the review paper [28]. The SQP method needs an initial estimate of the PSD, which we took to be the CLD. The SQP method converged in 2 min for 500 bins (a 1.0 GHz Pentium III processor was used for all computations). For the numerical example that follows, neither the penalty term nor the positivity constraint were needed, so the globally convergent Newton routine NEWT [26] was used to solve the system of nonlinear equations (Eq. (15)), which resulted in less computational expense. The calculation of the linear scale PSD using NEWT was accomplished in less than 1 min.

3. Numerical example

In order to compare the accuracy of the methods, each method is applied to a known PSD. In this case, the PSD (see Fig. 2) is described by the normal distribution function

$$f_{\mathrm{PSD}}(D) = \frac{1}{50\sqrt{2\pi}} \mathrm{e}^{-(1/2)((D-250)/50)^2} \tag{19}$$

The PSDs will be compared in terms of their j moments:

$$\mu_j = \int_0^\infty D^j f(D)\,\mathrm{d}D \tag{20}$$

The number mean particle size is defined by

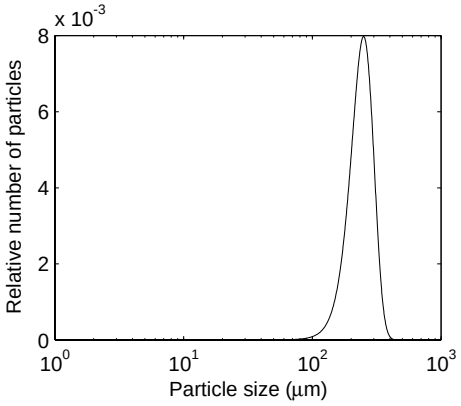

Fig. 2. The particle size distribution described by (19).

Table 1
The mean particle size, coefficient of variation, and moment ratios of the PSD described by (19)

$\bar{D}$ (μm)	250.00
cv	0.200
μ_2/μ_0 (μm^2)	6.5000×10^4
μ_3/μ_0 (μm^3)	1.7500×10^7
μ_4/μ_0 (μm^4)	4.8625×10^9

$$\bar{D} = \frac{\int_0^\infty D f(D)\,\mathrm{d}D}{\int_0^\infty f(D)\,\mathrm{d}D} = \frac{\mu_1}{\mu_0} \tag{21}$$

The coefficient of variation (cv), which quantifies the width of the distribution function relative to its mean, is defined by

$$\mathrm{cv} = \sqrt{\frac{\mu_0\mu_2}{\mu_1^2} - 1} \tag{22}$$

The mean particle size, coefficient of variation, and moment ratios of the PSD are in Table 1. The CLD is calculated by (4) where $\boldsymbol{P}$ is defined by

$$P_{ij} = \begin{cases} \dfrac{\int_{D_j}^{D_{j+1}} f_{\mathrm{PSD}}(D)(\sqrt{1-(D_i/D)^2} - \sqrt{1-(D_{i+1}/D)^2})\,\mathrm{d}D}{\int_{D_j}^{D_{j+1}} f_{\mathrm{PSD}}(D)\,\mathrm{d}D}, & i < j \\ \dfrac{\int_{D_j}^{D_{j+1}} f_{\mathrm{PSD}}(D)\sqrt{1-(D_i/D)^2}\,\mathrm{d}D}{\int_{D_j}^{D_{j+1}} f_{\mathrm{PSD}}(D)\,\mathrm{d}D}, & i = j \\ 0, & i > j \end{cases} \tag{23}$$

The CLDs are reported for the logarithmically distributed bins (see Fig. 3) and linearly distributed bins (see Fig. 4). The CLDs for the logarithmically distributed bins are noticably different, especially around the peak (see Fig. 3).

The three inverse modeling methods were applied to the CLDs computed from the PSD described in (19). The PSD was recovered from the CLD using the three inverse mod-

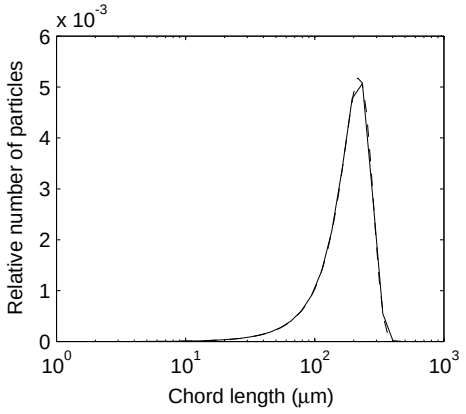

Fig. 3. The chord length distribution of (19) for 38 bins (—) and 90 bins (––). The bins are distributed logarithmically.

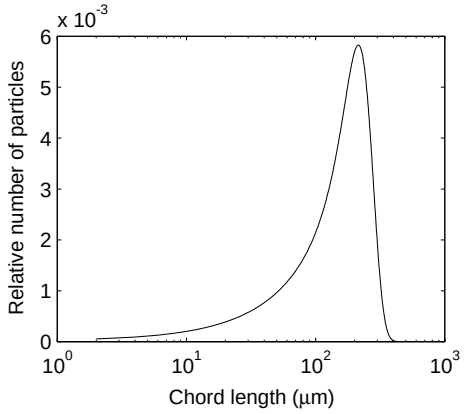

Fig. 4. The chord length distribution (19) for 500 bins (—). The bins are distributed linearly.

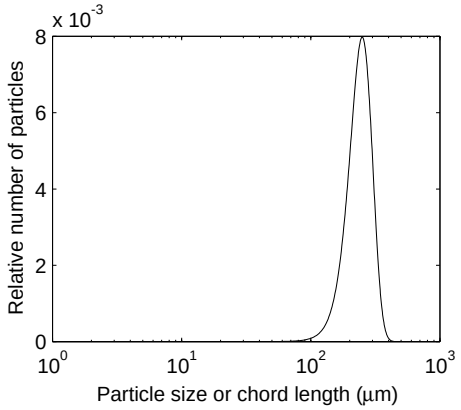

Fig. 5. The calculated PSD ($\hat{\gamma} = 0$) (—) using a linear distribution on a linear scale.

eling methods, with $\gamma = \hat{\gamma} = 0$ in (14) and (16) (nonzero values were not needed since there was no noise).

Table 2 reports the mean particle size, coefficient of variation, and the moment ratios for all the calculated PSDs. Not surprisingly, the PSDs calculated from the CLD with 38 bins were the least accurate, followed by the PSDs calculated from the CLD with 90 bins. What is more surprising is the magnitude of the relative accuracies of the three methods. For the logarithmically distributed bins, the midpoint method gave more accurate results than the uniform method, although the midpoint distribution might have been expected to be a poorer approximation to the PSD, since it assumes that the PSD consists of a series of spikes. All of the properties of the PSD calculated from 500 bins assuming a linear distribution within bins are accurate within five significant figures, whereas the midpoint and uniform methods only give two to three significant figures of accuracy when 500 bins are used. The PSD calculated from the linear method from the CLD with 90 bins is more accurate than the PSD calculated from the midpoint or uniform methods from the CLD with 500 bins.

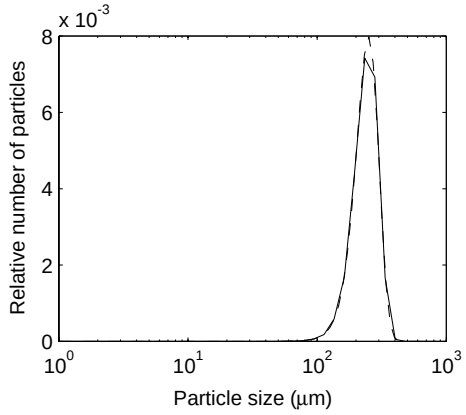

Fig. 6. The calculated PSD ($\hat{\gamma} = 0$) (38 channels (—) and 90 channels (– –)) using a linear distribution on a logarithmic scale.

The PSDs calculated assuming a linear distribution in each bin are reported in Figs. 5 and 6. The PSD calculated from 500 bins is nearly equal to the original PSD, whereas the PSD calculated from 38 bins is inaccurate near the peak.

Table 2
Comparison of the mean particle size ($\bar{D}$), coefficient of variation (cv), and moment ratios (μ_j) for the PSDs obtained from inverse modeling of (23) ($\gamma = \hat{\gamma} = 0$)

Method	$\bar{D}$ (μm)	cv	μ_2/μ_0 (μm^2)	μ_3/μ_0 (μm^3)	μ_4/μ_0 (μm^4)
500 linear bins					
Midpoint	251.00	0.199	6.5501×10^4	1.7696×10^7	4.9329×10^9
Uniform	251.00	0.199	6.5501×10^4	1.7696×10^7	4.9330×10^9
Linear	250.00	0.200	6.5001×10^4	1.7500×10^7	4.8627×10^9
38 logarithmic bins					
Midpoint	258.45	0.203	6.9557×10^4	1.9403×10^7	5.5908×10^9
Uniform	271.62	0.198	7.6671×10^4	2.2410×10^7	6.7637×10^9
Linear	252.12	0.211	6.6388×10^4	1.8175×10^7	5.1554×10^9
90 logarithmic bins					
Midpoint	247.67	0.212	6.4098×10^4	1.7235×10^7	4.7944×10^9
Uniform	259.50	0.199	7.0013×10^4	1.9554×10^7	5.6351×10^9
Linear	250.47	0.202	6.5302×10^4	1.7646×10^7	4.9254×10^9

4. Experimental procedure

The material used in this experiment was a reference sample supplied by Lasentec, which is 8.33 wt.% poly(vinyl chloride) (PVC) in water. The beaker was placed on the fixed beaker stand provided by Lasentec. The fixed beaker stand holds the FBRM probe stationary in the beaker, with a four blade turbine stirrer used to ensure that a slurry with a representative PVC size distribution passes towards the probe tip with an angle of approximately 45°. The stirring rate was 400 rpm. The FBRM software allows for fine (F)- and coarse (C)-electronics. The F-electronics is a more sensitive setting. F-electronics was used for all measurements. The measured CLD was highly reproducible (see Fig. 7). Also, the size distribution of PVC beads was constructed from the cumulative number distribution function for 278 particles

$$F(D) = \int_0^D f(D)\,\mathrm{d}D \tag{24}$$

whose size was measured by off-line optical microscopy (OM) (see Fig. 8). The percentage of particles of size less than or equal to D, $F(D)$, was calculated. This gives a monotonically nondecreasing staircase-like function to which a smooth curve is fitted. The number distribution is calculated by taking the derivative of this smooth curve

$$f(D) = \frac{\mathrm{d}F(D)}{\mathrm{d}D} \tag{25}$$

The mean particle size and coefficient of variation determined by off-line optical microscopy are reported in Table 3.

As a final comment, the measured CLDs reported in this paper are not a strong function of the suspension density. Increasing suspension density will cause incrementally less total particle counts at very high suspension densities, but this effect is canceled by using the normalized distributions used here. A secondary effect that can occur for particle sizes that range several orders-of-magnitude is that the smallest particles can "screen" the largest particles when there are very high numbers of small particles, leading to an undercounting of large particles. The particle sizes considered in this study range over a small enough range that this secondary effect is negligible.

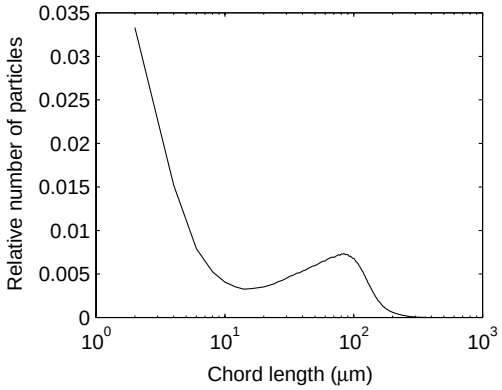

Fig. 7. The chord length distribution of PVC (linear scale).

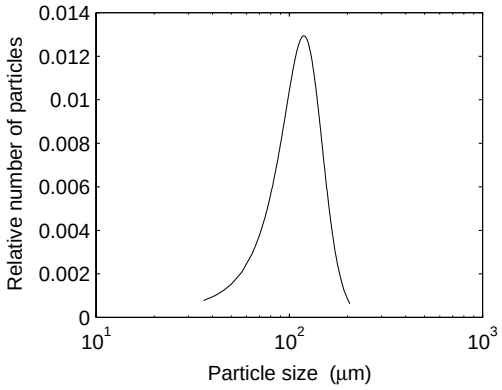

Fig. 8. The particle size distribution of PVC measured using off-line optical microscopy.

Table 3
The mean particle size, coefficient of variation, and moment ratios of PVC measured using off-line optical microscopy

Method	OM
$\bar{D}$ (μm)	119.05
cv	0.27
μ_2/μ_0 (μm^2)	1.52×10^4
μ_3/μ_0 (μm^3)	2.05×10^6
μ_4/μ_0 (μm^4)	2.90×10^8

5. Experimental results

The three inverse modeling methods were applied to the CLD data from the Lasentec FBRM. Three different bin grouping options were used. The linear bin grouping has 500 bins equally distributed over the range 0–1000 μm. The logarithmic bin grouping has 38 or 90 bins distributed over the range 1–1000 μm.

Properties of the calculated PSDs are reported for each method in Table 4. In each case, the method fails to accurately calculate the distribution of the PVC particles measured using off-line optical microscopy (as seen in Table 3). When applied to the CLD with 500 linear bins, the three methods underestimate the mean particle size. For logarithmic bins, the uniform method using 38 or 90 bins overestimates the mean particle size.

The PSDs calculated from the CLD assuming a linear distribution within bins are reported in Figs. 9 and 10. For linear bins, the second derivative term smoothes the fluctuations without greatly biasing the results.

All three methods with all three types of binning showed two peaks in the calculated PSD, whereas only the peak around 100 μm was observed in off-line optical microscopy. No polymer beads smaller than 10 μm were seen in the optical microscope; however, images of the polymer surface

Table 4
Comparison of the calculated mean particle size, coefficient of variation, and moment ratios from the PSDs calculated from inverse modeling of the CLD measured using FBRM

Method	$\bar{D}$ (μm)	cv	μ_2/μ_0 (μm^2)	μ_3/μ_0 (μm^3)	μ_4/μ_0 (μm^4)
500 linear bins					
Midpoint ($\gamma = 0$)	94.69	0.68	1.31×10^4	2.16×10^6	4.19×10^8
Midpoint ($\gamma = 0.1$)	98.11	0.73	1.47×10^4	2.78×10^6	6.52×10^8
Uniform ($\gamma = 0$)	94.73	0.68	1.31×10^4	2.16×10^6	4.19×10^8
Uniform ($\gamma = 0.1$)	98.11	0.73	1.47×10^4	2.77×10^6	6.48×10^8
Linear ($\hat{\gamma} = 0$)	95.72	0.66	1.32×10^4	2.17×10^6	4.22×10^8
Linear ($\hat{\gamma} = 0.1$)	95.91	0.66	1.32×10^4	2.17×10^6	4.20×10^8
38 logarithmic bins					
Midpoint ($\gamma = 0$)	94.79	0.67	1.30×10^4	2.13×10^6	4.09×10^8
Uniform ($\gamma = 0$)	138.45	0.44	2.29×10^4	4.47×10^6	1.02×10^9
Linear ($\hat{\gamma} = 0$)	108.98	0.50	1.49×10^4	2.46×10^6	4.89×10^8
90 logarithmic bins					
Midpoint ($\gamma = 0$)	95.32	0.67	1.32×10^4	2.17×10^6	4.20×10^8
Uniform ($\gamma = 0$)	138.46	0.44	2.29×10^4	4.45×10^6	1.01×10^9
Linear ($\hat{\gamma} = 0$)	113.45	0.49	1.60×10^4	2.73×10^6	5.53×10^8

collected by off-line optical microscopy showed protrusions up to 20 μm in size. On the other hand, CLDs collected from droplets and glass beads larger than 20 μm in the laboratory did not show any peaks in the 0–20 μm size range.

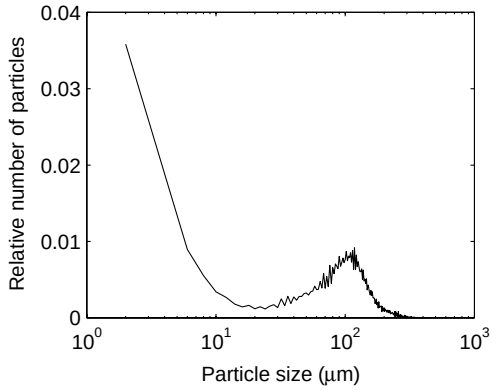

Fig. 9. The calculated PSD (—) using a linear distribution ($\hat{\gamma} = 0$). The bins are distributed linearly.

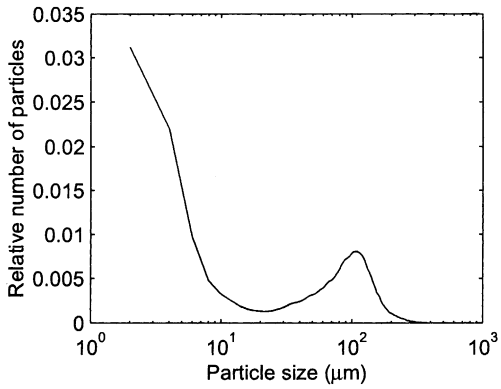

Fig. 10. The calculated PSD (—) using a linear distribution ($\hat{\gamma} = 0.1$). The bins are distributed linearly.

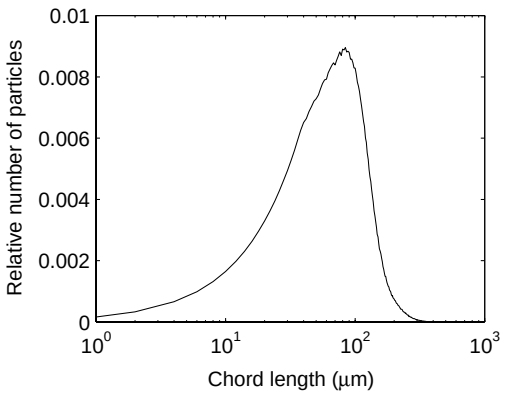

Fig. 11. The chord length distribution of PVC (linear scale) with surface roughness removed.

This suggests that the peak at 0–20 μm is caused by the laser interaction with the roughness/protrusions on the surface of the polymer beads, agreeing with a conclusion made in a previous study [36]. The next section describes a simple approach to take surface roughness into account in the inverse modeling step.

6. Surface roughness

Surface roughness is addressed by adjusting the CLD so that the prominent peak in the 0–20 μm is replaced with a linear equation (seen in Fig. 11)

$$c^{\text{surface}}(D) = \begin{cases} \dfrac{c^{\text{orig}}(D^\star) - c^{\text{orig}}(D_1)}{D^\star - D_1} \\ \quad \times (D - D_1) + c^{\text{orig}}(D_1), & D \le D^\star \\ c^{\text{orig}}(D), & D > D^\star \end{cases} \tag{26}$$

Table 5
Comparison of properties of the calculated PSDs from inverse modeling with surface roughness taken into account

Method	$\bar{D}$ (μm)	cv	μ_2/μ_0 (μm^2)	μ_3/μ_0 (μm^3)	μ_4/μ_0 (μm^4)
500 linear bins					
Midpoint ($\gamma = 0$)	117.88	0.43	1.65×10^4	2.73×10^6	5.29×10^8
Midpoint ($\gamma = 0.1$)	122.15	0.49	1.85×10^4	3.51×10^6	8.23×10^8
Uniform ($\gamma = 0$)	117.91	0.43	1.65×10^4	2.73×10^6	5.29×10^8
Uniform ($\gamma = 0.1$)	122.15	0.49	1.85×10^4	3.50×10^6	8.18×10^8
Linear ($\hat{\gamma} = 0$)	116.92	0.44	1.63×10^4	2.68×10^6	5.19×10^8
Linear ($\hat{\gamma} = 0.1$)	116.91	0.44	1.63×10^4	2.68×10^6	5.19×10^8
38 logarithmic bins					
Midpoint ($\gamma = 0$)	111.50	0.49	1.54×10^4	2.51×10^6	4.84×10^8
Uniform ($\gamma = 0$)	139.25	0.43	2.30×10^4	4.50×10^6	1.03×10^9
Linear ($\hat{\gamma} = 0$)	109.59	0.49	1.49×10^4	2.48×10^6	4.92×10^8
90 logarithmic bins					
Midpoint ($\gamma = 0$)	112.01	0.49	1.56×10^4	2.56×10^6	4.96×10^8
Uniform ($\gamma = 0$)	139.25	0.43	2.30×10^4	4.47×10^6	1.02×10^9
Linear ($\hat{\gamma} = 0$)	114.08	0.49	1.61×10^4	2.74×10^6	5.56×10^8

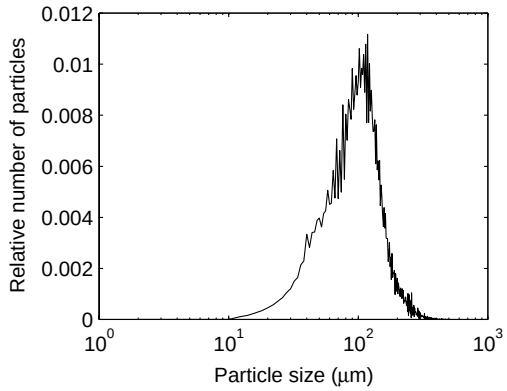

Fig. 12. The calculated PSD (—) using a linear distribution ($\hat{\gamma} = 0$). The bins are distributed linearly.

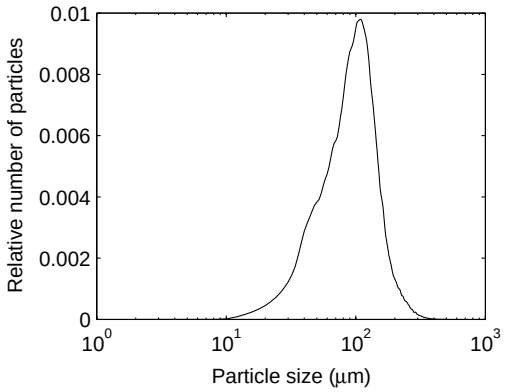

Fig. 13. The calculated PSD (—) using a linear distribution ($\hat{\gamma} = 0.1$). The bins are distributed linearly.

where $D^\star$ is the specified minimum particle diameter and D_1 is the diameter of the smallest bin (0 μm on linear scales and 1 μm on logarithmic scales). Then the three methods (midpoint, uniform, and linear) are applied to the modified CLDs. The PSDs calculated from the modified CLD using the linear methods are reported in Figs. 12 and 13. For linear bins, the nonzero $\hat{\gamma}$ or γ removes the oscillations with a small bias. The calculated PSDs are now unimodal, with a peak around 100 μm. The use of C-electronics is another remedy to remove the prominent peak in the 0–20 μm range.

Properties of the calculated PSDs are reported in Table 5. For linear bins, the calculated mean particle sizes for all the methods are all fairly close to the mean particle size determined by off-line optical microscopy. For logarithmic bins, the mean particle sizes are improved, but not as much as for the linear bins. In particular, the uniform method overestimates the mean particle size by as much as 20 μm. For 500 linear bins, all three methods give similar calculated PSD properties for $\gamma = \hat{\gamma} = 0$. However, nonzero γ was needed to give realistically smooth PSDs. For nonzero γ, many of the calculated PSD properties are significantly biased for the midpoint and uniform methods. Only the linear method with $\hat{\gamma} = 0.1$ gave both a smooth distribution *and* unbiased estimates of the PSD and its properties (with values similar to those obtained by off-line optical microscopy). Also, the linear method was much more robust to varying numbers of bins and to whether linear or logarithmic bins was used. *This provides strong support for using the linear method over past methods.*

7. Conclusions

This paper addresses the determination of the PSD based on the CLD measured using laser backscattering. Three distributions of particles within each bin were considered: midpoint, uniform, and linear. Each method was applied to a known distribution to compare their relative accuracies. The PSD calculated from the linear method was nearly two orders-of-magnitude more accurate than the PSD calculated from the widely accepted uniform and midpoint methods.

Then the three methods were applied to laser backscattering data collected from an aqueous suspension of poly(vinyl chloride) particles. A simple modification was proposed to the laser backscattering data to correct for the effect of surface roughness. With this correction, the linear method with a weight on the second derivative of the calculated PSD gave a smooth distribution that agreed very well with the PSD as measured from off-line optical microscopy. This in situ measurement of the PSD should enable significant advances in the modeling and control of suspension polymerization reactors.

References

[1] T. Allen, Particle Size Measurement, Chapman & Hall, London, fourth ed., 1990.

[2] P. Barrett, B. Glennon, In-line FBRM monitoring of particle size in dilute agitated suspensions, Part. Part. Syst. Charact. 16 (1999) 207–211.

[3] R.D. Braatz, S. Hasebe, Particle size and shape control in crystallization processes, in: J.B. Rawlings, B.A. Ogunnaike, J.W. Eaton (Eds.), Proceedings of the Sixth International Conference on Chemical Process Control, AIChE Symposium Series, vol. 98, AIChE Press, New York, 2002, pp. 307–327.

[4] K. Cao, J. Yu, B. Li, B. Li, Z. Pan, Micron-size uniform poly(methyl methacrylate) particles by dispersion polymerization in polar media. 1. Particle size and particle size distribution, Chem. Eng. J. 78 (2000) 211–215.

[5] E.G. Chatzi, C.J. Boutris, C. Kiparissides, On-line monitoring of drop size distributions in agitated vessels, Ind. Eng. Chem. Res. 30 (1991) 1307–1313.

[6] E.G. Chatzi, C. Kiparissides, Steady-state drop size distributions in high holdup fraction dispersion systems, AIChE J. 41 (1995).

[7] F. Chu, J. Guillot, A. Guyot, Study of poly(St/BA/MAA) copolymer latexes with bimodal particle size distribution, Polym. Adv. Technol. 9 (1998) 851–857.

[8] M.F. Cunningham, Microsuspension polymerization of methyl methacrylate, Polym. React. Eng. 7 (1999) 231–257.

[9] P.J. Dowding, J.W. Goodwin, B. Vincent, Production of porous suspension polymers using a continuous tubular reactor, Colloid Polym. Sci. 278 (2000) 346–351.

[10] P.J. Dowding, J.W. Goodwin, B. Vincent, Factors governing emulsion droplet and solid particle size measurements performed using the focused beam reflectance technique, Colloids Surf. A: Physicochem. Eng. Aspects 192 (2001) 5–13.

[11] P.J. Dowding, J.W. Goodwin, B. Vincent, Production of porous suspension polymer beads with a narrow size distribution using a cross-flow membrane and a continuous tubular reactor, Colloids Surf. A: Physicochem. Eng. Aspects 180 (2001) 301–309.

[12] R. Eek, Control and dynamic modeling of industrial suspension crystallizers, Ph.D. thesis, Delft University of Technology, The Netherlands, 1991.

[13] R.A. Eek, S. Dijkstra, Design and experimental evaluation of a state estimator for a crystallization process, Ind. Eng. Chem. Res. 34 (1995) 567–574.

[14] R.J. Farrell, Y.-C. Tsai, Nonlinear controller for batch crystallization: development and experimental demonstration, AIChE J. 41 (1995) 2318–2321.

[15] FDS Research, 2003 (http://www.fdsresearch.com).

[16] R. Gunawan, D.L. Ma, M. Fujiwara, R.D. Braatz, Identification of kinetic parameters in a multidimensional crystallization process, Int. J. Modern Phys. B 16 (2002) 367–374.

[17] J. Jager, S. de Wolf, W. Klapwijk, E.J. de Jong, A new design for on-line product-slurry measurements, in: Industrial Crystallization, vol. 87, 1987, pp. 415–418.

[18] O. Kammona, E.G. Chatzi, C. Kiparissides, Recent developments in hardware sensors for the on-line monitoring of polymerization reactions, Rev. Macromol. Chem. Phys. 39 (1999) 57–134.

[19] Lasentec, 2003 (http://www.lasentec.com).

[20] D.-H. Lee, Correlation on the mean particle diameter of PVC resin in VCM suspension polymerization, J. Chem. Eng. Jpn. 32 (1999) 97–103.

[21] W. Liu, N.N. Clark, A.I. Karamavruc, Relationship between bubble size distributions and chord-length distribution in heterogeneously bubbling systems, Chem. Eng. Sci. 53 (1998) 1267–1276.

[22] O. Monnier, J.-P. Klein, C. Hoff, B. Ratsimba, Particle size determination by laser reflection: methodology and problems, Part. Part. Syst. Charact. 13 (1996) 10–17.

[23] A. Pankewitz, H. Geers, In-line crystal size distribution analysis in industrial crystallisation processes by ultrasonic extinction, Technical report, Sympatec GmbH, System-Partikel-Technik, Clausthal-Zellerfeld, Germany, 2003.

[24] G. Polacco, C. Basile, M. Palla, D. Semino, A simple technique for measuring particle size distributions during suspension polymerization, Polym. J. 32 (2000) 688–693.

[25] G. Polacco, M. Palla, D. Semino, Measurements of particle size distribution during suspension polymerization, Polym. Int. 48 (1999) 392–397.

[26] W.H. Press, S.A. Teukolsky, W.T. Vetterling, B.P. Flannery, Numerical Recipes in FORTRAN: The Art of Scientific Computing, second ed., Cambridge University Press, London, 1992.

[27] A.D. Randolph, E.T. White, C.-C.D. Low, On-line measurement of fine-crystal response to crystallizer disturbances, Ind. Eng. Chem. Proc. Des. Dev. 20 (1981) 496–503.

[28] J.B. Rawlings, S.M. Miller, W.R. Witkowski, Model identification and control of solution crystallization processes: a review, Ind. Eng. Chem. Res. 32 (1993) 1275–1296.

[29] J.L. Reimers, F.J. Schork, Predominant droplet nucleation in emulsion polymerization, J. Appl. Polym. Sci. 60 (1996) 251–262.

[30] R.D. Rovang, A.D. Randolph, On-line particle size analysis in the fines loop of a KCl crystallizer, in: A.D. Randolph (Ed.), Design, Control, and Analysis of Crystallization Processes, vol. 76, AIChE Symposium Series No. 193, AIChE, New York, 1980, pp. 18–26.

[31] A. Ruf, J. Worlitschek, M. Mazzotti, Modeling and experimental analysis of PSD measurements through FBRM, Part. Part. Syst. Charact. 17 (2000) 167–179.

[32] A. Tadayyon, S. Rohani, Determination of particle size distribution by Par Tec 100: modeling and experimental results, Part. Part. Syst. Charact. 15 (1998) 127–135.

[33] T. Tahti, M. Louhi-Kultanen, S. Palosaari, On-line measurement of crystal size distribution during batch crystallization, in: Proceedings of the 14th International Symposium Industrial Crystallization, Institution of Chemical Engineers, Rugby, UK, 1999, pp. 1–9.

[34] E. Vivaldo-Lima, P.E. Wood, A.E. Hamielec, A. Penlidis, An updated review on suspension polymerization, Ind. Eng. Chem. Res. 36 (1997) 939–965.

[35] S. Wang, G. Poehlein, F. Schork, Miniemulsion polymerization of styrene with chain transfer agent as cosurfactant, J. Polym. Sci. Part A: Polym. Chem. 35 (1997) 595–603.

[36] J. Worlitschek, T. Hocker, M. Mazzotti, Monitoring of particle size distribution using Lasentec FBRM, in: Lasentec Users Forum, 2002 (http://www.lasentec.com).

[37] J.L. Zhou, A.L. Tits, C.T. Lawrence, User's Guide for FFSQP Version 3.7: A FORTRAN Code for Solving Constrained Nonlinear (Minmax) Optimization Problems, Generating Iterates Satisfying All Inequality and Linear Constraints, Electrical Engineering Department and Institute for Systems Research, University of Maryland, College Park, MD, April 1997.